

# Seismic response analysis of isolated offshore bridge with friction sliding bearings

Baofu Wang<sup>1,2</sup>, Qiang Han<sup>\*1</sup> and Junfeng Jia<sup>1</sup>

<sup>1</sup>Key Laboratory of Urban Security and Disaster Engineering of Ministry of Education, Beijing University of Technology, Beijing, China  
<sup>2</sup>Department of Civil Engineering, North China Institute of Science and Technology, Hebei, China

(Received October 18, 2018, Revised March 22, 2019, Accepted March 26, 2019)

**Abstract.** This paper investigates the seismic response of a typical non-navigable continuous girder bridge isolated with friction sliding bearings of the Hong Kong-Zhuhai-Macao link projects in China. The effectiveness of the friction pendulum system (FPS) and accuracy of the numerical model were evaluated by a 1/20 scaled bridge model using shaking table tests. Based on the hysteretic properties of friction pendulum system (FPS), double concave friction pendulum (DCFP), and triple friction pendulum system (TFPS), seismic response analyses of isolated bridges with the three sliding-type bearings are systematically carried out considering soil-pile interaction under offshore soft clay conditions. The fast nonlinear analysis (FNA) method and response spectrum are employed to investigate the seismic response of isolated offshore bridge structures. The numerical results show that the implementation of the three sliding-type bearings effectively reduce the base shear and bending moment of the reinforced concrete pier, at the cost of increasing the absolute displacement of the bridge superstructure. Furthermore, the TFPS and DCFP bearings show better isolation effect than FPS bearing for the example continuous girder bridge.

**Keywords:** friction sliding bearing; offshore bridge; seismic response; hysteretic model; isolation effect

## 1. Introduction

With the rapid development of China's economy, transport infrastructure such as offshore bridges need to be constructed in the coastal area of southeast China, most of which are located in moderate or high seismic regions on the Chinese seismic hazard map. Some highway bridges that have followed the seismic design codes and specifications suffered severe bearing damages or even unseating of the superstructures during the 2008 Wenchuan earthquake in China (Han *et al.* 2009), which highlights the poor displacement capacity of the bridge bearings. Bridge bearings are vulnerable components when bridge structures subject to earthquake excitations, therefore the seismic performance of bridge bearings have been investigated extensively (Han *et al.* 2012, Peng and Wu 2017). Currently, there are two seismic design approaches available for reducing destructive effects caused by strong earthquakes. One is to use isolation device, which is a strategy that attempts to reduce the seismic forces to near the elastic capacity of structural members, thereby eliminating or reducing the inelastic deformations. The main concept of isolation is to reduce the fundamental frequency of structural vibration to a value lower than the predominant energy-containing frequencies of the earthquake. The other is to use energy dissipation device or increase damping, which is intended to reduce seismic

energy input into the structure. Therefore, it is possible to control large plastic deformations caused by the natural period elongation. Both these beneficial effects are typically realized by using non-linear devices, which can ensure a minimum required linear horizontal stiffness under small deformations. This stiffness decreases due to nonlinear response, decoupling deck from pier under strong seismic events, and then increasing protection efficiency.

Laminated rubber bearings, such as the high damping rubber bearing (HDRB) system and the lead rubber bearing (LRB) system, have been extensively used in seismic isolation system. However, the mechanical property of rubber bearings makes them vulnerable to marine erosion environment and the future replacement is very difficult due to the heavy weight of the superstructure in offshore bridges. Therefore, the sliding bearings, which have high bearing capacity and favorable durability (Castaldo *et al.* 2015), provide a better solution for bridge seismic isolation system. The sliding isolators can be generally classified into three categories: (1) the friction pendulum system (FPS), which was proposed by Zayas *et al.* (1987) and has been proved to be an efficient device in reduction of the seismic responses of structures (Saha *et al.* 2018, Castaldo *et al.* 2015) (2) the double concave friction pendulum (DCFP), which was introduced by researchers (Constantinou 2004, Fenz and Constantinou 2006). The seismic response characteristics of structures with DCFP bearings have been reported by Kim and Yun (2007) and Faramarz and Montazar (2010). (3) the triple friction pendulum system (TFPS), which has four or more sliding surfaces as well as adaptive stiffness and damping properties, is especially suitable for being incorporated with performance based

\*Corresponding author, Professor  
E-mail: qhan@bjut.edu.cn



Fig. 1 The bridge in construction

seismic design (Billah and Alam 2016, Catalán and Foti 2015). Fenz and Constantinou (2008a, b), Fadi and Constantinou (2010) investigated the mechanical behavior and the series model of TFPS with four sliding surfaces. Tsai *et al.* (2006, 2010) established the lateral force-displacement relationship of the bearing with numerous concave sliding interfaces through experimental research. Han *et al.* (2012) developed the multi-spherical sliding friction isolation bearings to meet the requirement of offshore bridges in high seismic regions for isolation bearings. Amiri *et al.* (2016) proposed a direct displacement-based design procedure for a continuous deck bridge isolated with triple friction pendulum bearings.

The seismic response of a typical non-navigable continuous girder bridge isolated with friction sliding bearings in the Hong Kong-Zhuhai-Macao link projects of China was investigated in this paper. The effectiveness of FPS and accuracy of the numerical model were evaluated by a 1/20 scaled bridge model using shaking table tests results by Du *et al.* (2016), Kang *et al.* (2014). The seismic response analyses of isolated bridges with three sliding-type of bearings were carried out considering soil-pile interaction under offshore soft clay conditions based on hysteretic properties of FPS, DCFP, and TFPS. The fast nonlinear analysis (FNA) method and response spectrum analysis were employed to investigate seismic response of the isolated offshore bridge structures. Hysteretic characteristics and seismic isolation effect of the three types of bearings were compared to provide reference for bridge seismic isolation design.

## 2. Description of the Non-navigable Bridge

The examined offshore bridge is a typical continuous girder bridge in the Hong Kong-Zhuhai-Macao link projects of China. In the shallow water non-navigable region, a multi-span composite continuous girder bridge is adopted. The arrangement of the non-navigable bridge is  $6 \times 85000$  mm as one continuous unit, as shown in Fig. 1.

The composite single-cell box girders with a deck width

of 16300 mm and a deck height of 4300 mm are used for the example bridge. The composite girder consists of open-topped steel trough and top slab made of C60 marine durable concrete, which are tied together by shear connectors on top flange plates of the steel trough and small longitudinal girder. Truss diaphragm is used for the composite girder and there is one web stiffening rib between the adjacent diaphragms. Cross section of the bridge is shown in Fig. 2.

The plane dimension of the bent cap is  $23500 \text{ mm} \times 4000$  mm. Hollow section with thin-wall is adopted for the bridge pier. The external dimension of the pier is  $11000 \text{ mm} \times 3500$  mm and the thickness of the wall varies from 1200 to 1700 mm. The dimensions of the pier are as shown in Fig. 3. Prefabricated cushion caps and piers are used to construct the bridge substructure. The bridge is equipped with four bearings at each pier location for a total of 28 bearings. The bearings are directly located above the bent cap of the thin-wall columns.

Composite steel tube piles are utilized for the foundation. The pile length ranges from 4500 mm to 35500 mm, and 6 piles are employed for each pier. Diameter of the steel tube is 2000 mm, and dimension of the cushion cap is  $15600 \text{ mm} \times 11400$  mm. Low pier regions, where the height of the pier is 23750 mm and the length of the pile is 20000 mm, are selected for investigation in this paper.

## 3. Friction pendulum bearing

### 3.1 Friction pendulum system (FPS)

The friction pendulum system consists of a spherical stainless steel surface, an articulated slider and a housing plate, as shown in Fig. 4(a). Based on the working mechanisms and dynamic equilibriums, the force-displacement relationship and natural period of the FPS bearing are given by Eq. (1) and Eq. (2), the first term of the right hand side of Eq. (1) represents the restoring force mechanism related to the curvature of the sliding surface.

$$F = \frac{W}{R_{eff}} d + \mu W \text{sgn}(\dot{\theta}) \quad (1)$$

$$T = 2\pi \sqrt{R_{eff}/g} \quad (2)$$

where  $W$  is the vertical load,  $R_{eff}$  is the equivalent radius of the sliding surface ( $R_{eff} = R - h$ , where  $R$  is the radius of the concave and  $h$  is part height of the articulated slider),  $d$  is the relative displacement,  $\mu$  is the friction coefficient between the sliding surfaces,  $\dot{\theta}$  is the sliding velocity,  $\text{sgn}$  is the signum function. Eq. (2) shows that the natural period of vibration is independent of the mass of the superstructure.

### 3.2 Double concave friction pendulum (DCFP)

The double concave friction pendulum bearings as shown in Fig. 4(b) are made of two concave surfaces, which are called upper concave surface and lower concave surface, respectively. The friction coefficients ( $\mu_1, \mu_2$ ) of the

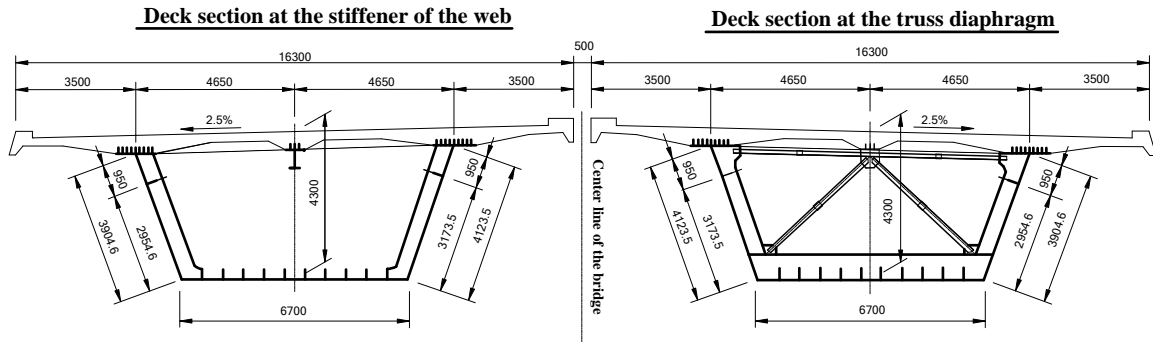


Fig. 2 Cross section of the bridge (Unit: mm)

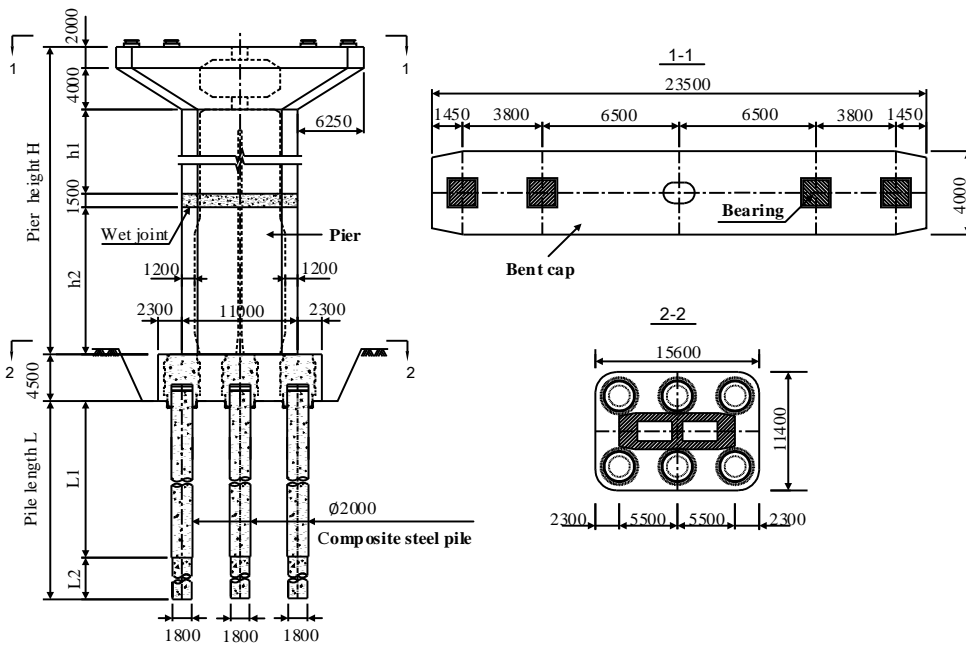


Fig. 3 Structure diagram of the pier (Unit: mm)

two concave surfaces were taken with different values. The restoring force and natural period of the DCFP bearing are given by the following equations (Constantinou 2004, Fenz and Constantinou 2006)

$$F = \frac{W}{R_{eff1} + R_{eff2}} d + \frac{f_1 R_{eff1} + f_2 R_{eff2}}{R_{eff1} + R_{eff2}} \quad (3)$$

$$T = 2\pi \sqrt{(R_{eff1} + R_{eff2}) / g} \quad (4)$$

Where  $R_{eff1}$  and  $R_{eff2}$  are the equivalent radii of the two sliding surfaces,  $f_1$  and  $f_2$  are the friction force of the two sliding surfaces.

### 3.3 Triple friction pendulum system (TFPS)

The triple friction pendulum system consists of two facing concave stainless steel surfaces separated by an internal nested slider assembly, which is made of two concave slide plates separated by a rigid slider, as shown in Fig. 4(c). TFPS has four sliding concave surfaces with the radii  $R_1=R_4$  and  $R_2=R_3$ , and four coefficients of friction. These bearings are fully passive devices that exhibit

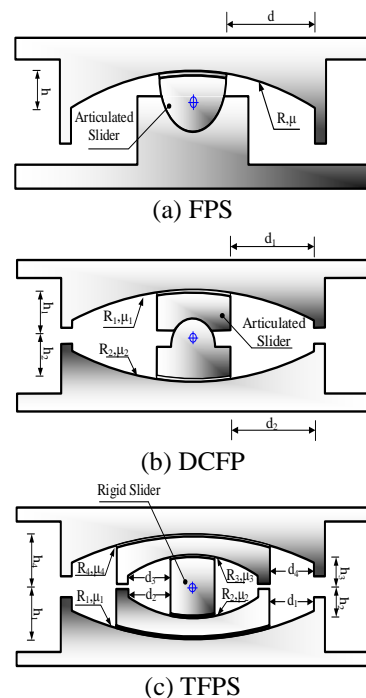


Fig. 4 Cross section of the three bearings

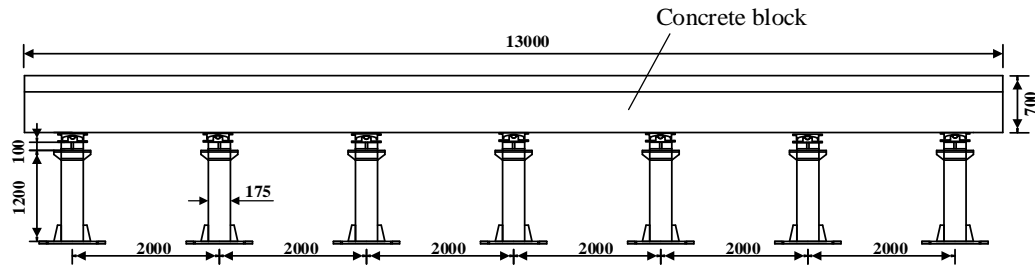


Fig. 5 The elevation drawing of the bridge model (unit: mm)



(a) The scaled bridge model

(b) FPS bearing

Fig. 6 Shake table test setup

Table 1 Similarity relation between model and prototype

Physical quantity	Similarity ratio	Physical quantity	Similarity ratio
length	1/20	acceleration	1.0
time	$1/\sqrt{20}$	velocity	$1/\sqrt{20}$
stress	1.0	displacement	1/20
weight	1/400	density	20

adaptive stiffness and damping behavior, which results from the internal construction of the bearings. The force-displacement relationship of the bearing is established, according to the dynamic equilibrium and geometrical relationship of the sliding surfaces, and the mechanical properties are shown in literatures (Fenz and Constantinou 2008a, b).

#### 4. Experimental investigation of the bridge isolated with FPS

To investigate the seismic response characteristics of the prototype offshore bridge isolated by FPS, a scaled bridge model was constructed and tested using shaking table tests (Du *et al.* 2016, Kang *et al.* 2014), as shown in Fig. 5 and Fig. 6. The scaled bridge model was then reused and tested with ordinary bearings as the benchmark model. The scaled bridge is 13 m long and has 6 spans with a spacing of 2 m. The focus of the test is the mechanical behavior of the isolation bearing, hence steel tube piers which remain within the elastic range during the test were utilized to preclude the influence from potential damage of reinforced concrete piers. Since the bridge deck is expected to exhibit rigid-body motion under horizontal excitations, the mass similarity is the main requirement for the deck model. Reinforced concrete blocks are placed on the top of girder, resulting in a total weight of 473.0 kN for the deck model.

Considering the shake table capacity, a scaling factor of 1/20 is used for the bridge model. Similarity relation between the model and prototype is given in Table 1. The horizontal ground motion recorded from San Fernando earthquake was compressed in time by a factor of  $1/\sqrt{20}$  to satisfy the similitude requirements of the shake table test, as shown in Fig. 7(a). Numerical model of the shake table test is established. Experimental and numerical results of the center pier are shown in Figs. 7(b)-(e).

Fig. 7(b) shows the experimental and numerical hysteretic loops of the FPS isolation system, which matches with the theoretical one well and shows the desired mechanical properties as described in section 3.1. Figs. 7(c)-(d) compares the shear responses of the bridge piers with and without FPS isolation system. The maximum shear force of the non-isolated bridge pier is 54.85 kN whereas that of the isolated bridge pier is 5.83 kN. Shear force ratio between the isolated and non-isolated bridge pier is approximately 1/3.27~1/9.41, indicating the effectiveness of the FPS bearing. Displacement responses of the bridge girder to pier top is shown in Fig. 7(e). The mean displacement value of FPS bearing under severe earthquake ranges from 1.628 to 3.56 cm, satisfying the displacement restriction, while the relative displacement of the pier top ranges from 1.364 to 3.981 cm, verifying that the bridge pier remain in elastic stage. From Figs. 7(b)-(e), it can be seen that the numerical results agree well with the test results.

#### 5. Finite element model of the bridge

##### 5.1 Modeling of bridge structure

Shake table tests verify the effectiveness of FPS bearing and the accuracy of the numerical model. Based on shake table test results, finite element model of the whole isolated

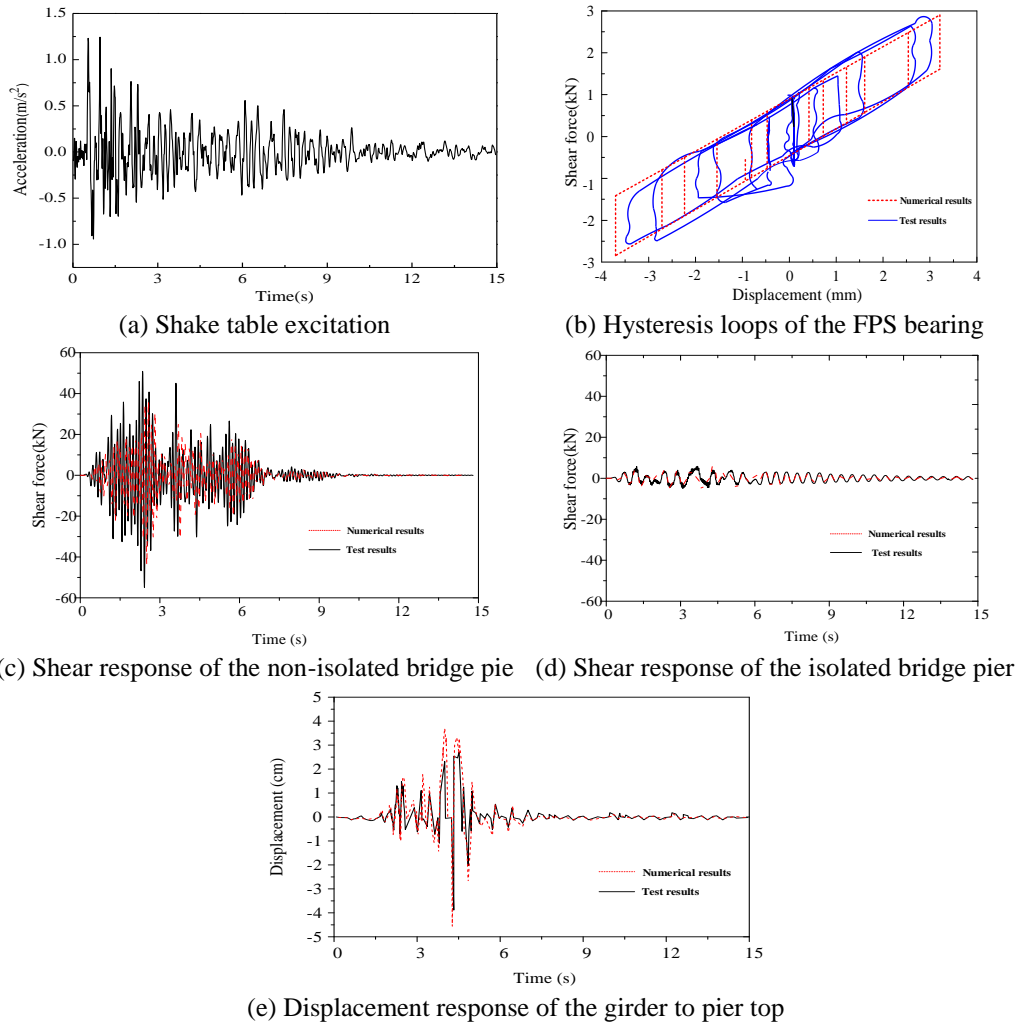


Fig. 7 Shake table test

prototype bridge is established to comprehensively investigate isolation effect of the three sliding-type bearings. The base isolation system aims to reduce the earthquake response to keep the bridge in the elastic range. Hence, the bridge superstructure, piers and pile foundation are assumed to remain in the elastic state during the earthquake excitation. Both the superstructure and substructure of the offshore bridge are modelled by elastic frame elements to improve computational efficiency. The mass of the element is assumed to be distributed between the two adjacent nodes in the form of point mass. The effect of non-structural elements to the stiffness of the bridge girder is neglected.

### 5.2 Modelling of friction sliding bearings

As the earthquake response of the isolated bridge is greatly influenced by the type of sliding isolators, particular attention is paid to the simulation of the mechanical behavior of the isolators. The Friction pendulum isolator and Gap elements are employed to model the three types of bearings. The Friction pendulum isolator in the commercial software SAP2000 is a biaxial hysteretic element for two shear deformations in horizontal directions. The post-elastic

Table 2 The property of each element in the series model of DCFP bearing

Series bearing	Friction coefficient	Equivalent radius	Rate parameter
FPS <sub>1</sub>	$\mu_{m1} = \mu_1$	$R_{m1} = R_{eff1}$	$a_{m1} = a_1$
FPS <sub>2</sub>	$\mu_{m2} = \mu_2$	$R_{m2} = R_{eff2}$	$a_{m2} = a_2$

stiffness of the FP element in two shear directions can be computed using the radius of curvature of the sliding surface considered whereas the uncoupled gap element is assigned to the axial direction. Linear properties of the FP element are only used for translational deformations.

The FP element is used to simulate the behavior of FPS bearings. As for DCFP bearing, under the condition of  $\mu_1 < \mu_2$  and  $R_{eff1} = R_{eff2}$ , considering structural relationship with FPS bearing, a series model of two FP elements is employed to simulate its mechanical properties, as shown in Fig. 8(a). The parameters of each element in the series model of DCFP bearing is given in Table 2. A series model of three FP elements is utilized to model TFPS bearing (Fenz and Constantinou 2008c), and the displacement restrainer is modeled by a GAP element, as depicted in Fig. 8(b). The property of each element in the series model of TFPS

Table 3 The property of each element in the series model of TFPS bearing

Series bearing	Friction coefficient	Equivalent radius	Displacement limit	Rate parameter
FPS <sub>1</sub>	$\mu_{m1} = \mu_2 = \mu_3$	$R_{m1} = R_{eff1} + R_{eff2}$	$D_{m1} = \sum_1^4 D_i - D_{m2} - D_{m3}$	$a_{m1} = \frac{a_2 + a_3}{4}$
FPS <sub>2</sub>	$\mu_{m2} = \mu_1$	$R_{m2} = R_{eff1} - R_{eff2}$	$D_{m2} = \frac{R_{eff1} - R_{eff2}}{R_{eff1}} D_1$	$a_{m2} = \frac{R_{eff1}}{R_{eff1} - R_{eff2}} a_1$
FPS <sub>3</sub>	$\mu_{m3} = \mu_4$	$R_{m3} = R_{eff4} - R_{eff2}$	$D_{m3} = \frac{R_{eff4} - R_{eff3}}{R_{eff4}} D_4$	$a_{m3} = \frac{R_{eff4}}{R_{eff4} - R_{eff3}} a_4$

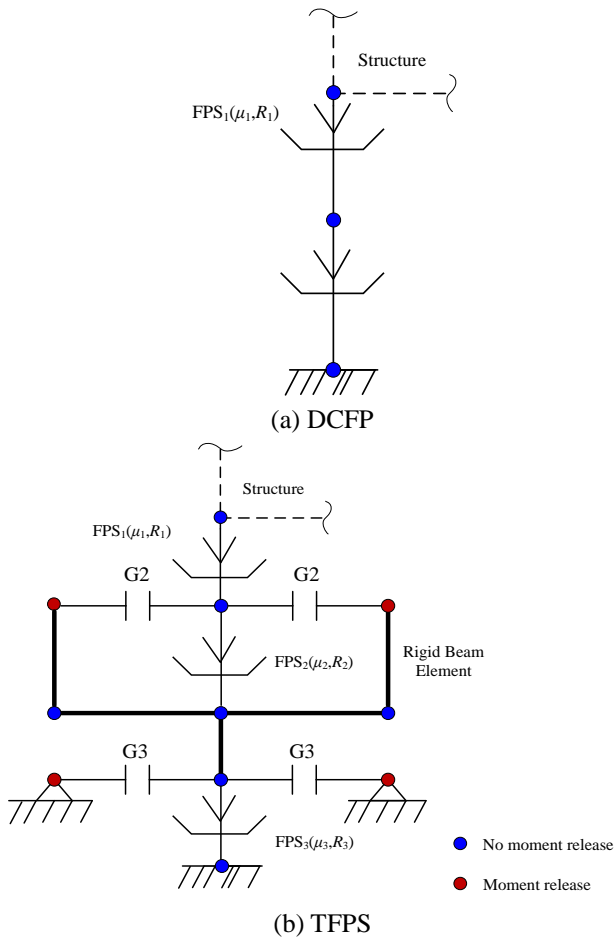


Fig. 8 The series models of bearings

bearing is given in Table 3.

In Tables 2 and 3,  $\mu_{mi}$ ,  $R_{mi}$ ,  $a_{mi}$ ,  $D_{mi}$  are the friction coefficient, equivalent radius, rate parameter and displacement limit, of the  $i$ th spherical surface for the series model, and  $\mu_i$ ,  $R_i$ ,  $a_i$ ,  $D_i$  are the friction coefficient, equivalent radius, rate parameter and displacement limit, of the  $i$ th spherical surface for the actual bearing, respectively.

With reference to the design documents, the fundamental vibration period of the isolated non-navigable bridge is approximate 2.5 s, hence the effective radius,  $R_{eff}=1550$  mm, is selected to yield a pendulum period equal to 2.5 s (Eq. (2)) and the friction coefficient is set to be 0.1. The dimension, radius and maximum friction coefficient of DCFP and TFPS bearings are identical to the FPS bearings and basic parameters of the three bearings are summarized in Table 4.

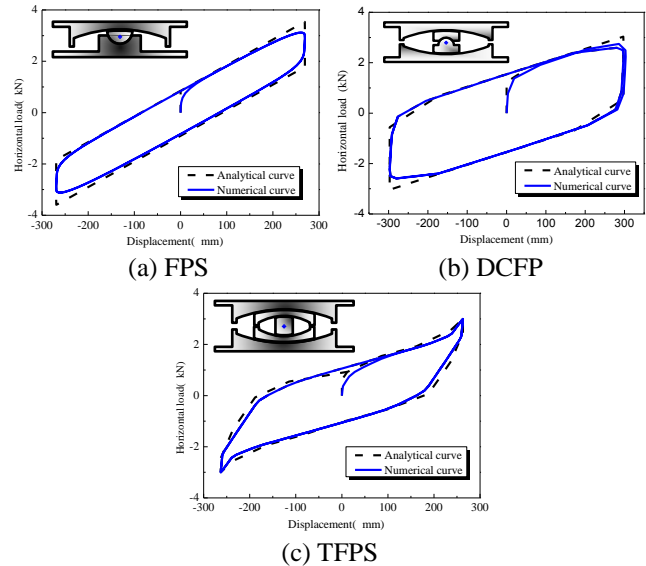


Fig. 9 The force-displacement relationship of bearings

To verify the aforementioned modeling techniques, quasi-static analyses were conducted. The analysis was carried out by fixing the bottom node and imposing a sinusoidal displacement history to the top node. The loops shown have displacement amplitudes corresponding to the displacement capacities of the three curved sliding devices. Displacement capacities of FPS, DCFP and TFPS are 270 mm, 300 mm and 270 mm respectively. Comparison of the force-displacement relationship between numerical and analytical analysis is shown in Fig. 9, where a good agreement is found.

### 5.3 Soil-pile interaction

Nonlinear Winkler foundation approach (Heidari *et al.* 2014) was adapted to model the soil-pile interaction, where beam-column elements represent the piles and nonlinear  $p$ - $y$  springs represent the soil, as shown in Fig. 10. The  $p$ - $y$  springs were used to simulate the lateral confinements in both transverse and longitudinal directions. Because the dynamic behavior of a continuous bridge system is mostly excited in the horizontal direction, the friction between the soil and pile was not taken into consideration and pinned connections were used at the bottom of piles.

The  $p$ - $y$  elements in clay followed the relationships developed by Matlock (1970). The lateral soil resistance-deflection ( $p$ - $y$ ) relationships for sand followed the API (2000). The following equations are used to determine the

Table 4 The basic parameter values of bearings

Type	Height $h_i$ (mm)	Radius $R_{eff}$ (mm)	Nominal displacement (mm)	Friction coefficient $\mu$	Rate parameter $a$ (sec/m)
FPS	$h=200$	$R_{eff}=1550$	$d=270$	$\mu=0.06-0.1$	0.1
DCFP	$h_1=h_2=100$	$R_{eff1}=R_{eff2}=1550$	$d_1 d_2=150$	$\mu_1=0.03-0.06, \mu_2=0.06-0.1$	0.1
TFPS	$h_1=h_4=100$ $h_2=h_3=50$	$R_{eff1}=R_{eff4}=1550$ $R_{eff2}=R_{eff3}=350$	$d_1=d_4=100$ $d_2=d_3=35$	$\mu_1=0.03-0.06$ $\mu_2=\mu_3=0.02-0.04$ $\mu_4=0.06-0.1$	0.1

\*The first value of friction coefficient  $\mu$  is for slow velocity and the second value for fast velocity.

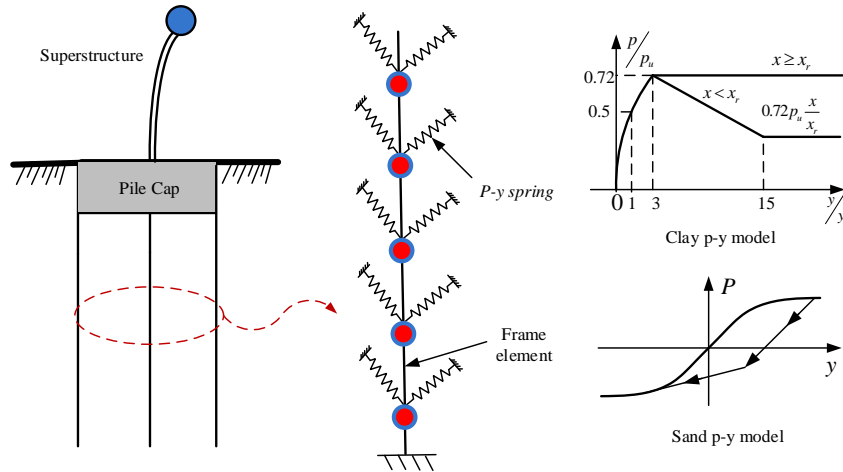


Fig. 10 The pile-soil interaction model

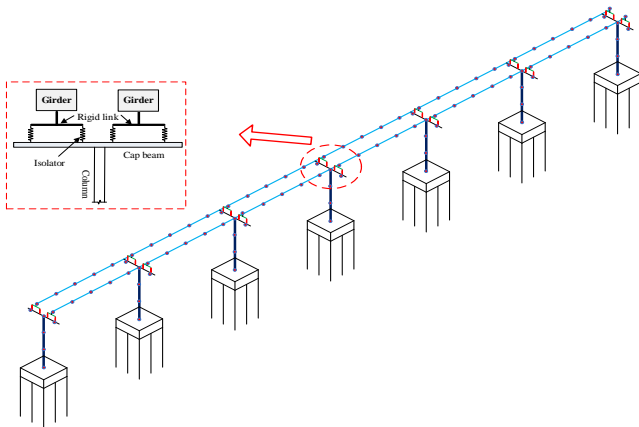


Fig. 11 Finite element model of the isolated bridge

Table 5 The basic soil parameters

Depth (m)	Soil type	Parameters
0-5	Silt	$k=17.74 \text{ kN/m}^3, C_1=3.01, C_2=3.45, C_3=28, \gamma=16.3 \text{ kN/m}^3$
5-13	Clay	$C=30 \text{ MPa}, \epsilon_{s0}=0.025, \gamma=18.5 \text{ kN/m}^3, J=0.25$
13-20	Sand	$k=5 \text{ kN/m}^3, C_1=3.01, C_2=3.45, C_3=28, \gamma=20.3 \text{ kN/m}^3$

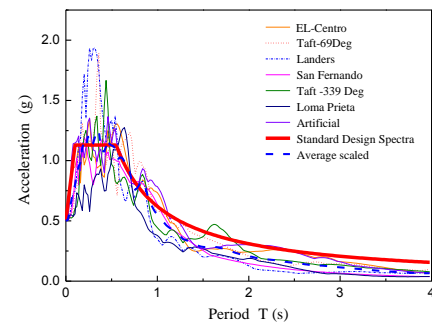


Fig. 12 Response spectrum of selected ground motions

relationships for sand.

$$p_{us} = (C_1 \times H + C_2 \times D) \times \gamma \times H \quad (5)$$

$$p_{ud} = C_3 \times D \times \gamma \times H \quad (6)$$

$$p_u = \min \{ p_{us}, p_{ud} \} \quad (7)$$

$$P = A \times p_u \times \tanh \left[ \frac{k \times H}{A \times p_u} \times y \right] \quad (8)$$

where  $P_{us}$  is the ultimate lateral bearing capacity of sand determined by shallow depths,  $P_{ud}$  is the ultimate lateral bearing capacity of sand determined by deep depths.  $\gamma$  is effective unit weight of soil.  $D$  is the average pile diameter

from top to the bottom.  $H$  is the depth of sand.  $C_1, C_2, C_3$  are coefficients determined by API (2000).  $P_u$  is the lower value of  $P_{us}$  and  $P_{ud}$  which should be used as the ultimate bearing capacity at depth  $H$ .  $A$  is the factor for cyclic loading condition.  $k$  is the initial modulus of subgrade reaction.  $y$  is the lateral deflection of sand.

The pile length of the offshore bridge is 20000 mm and the diameter of the pile is 2000 mm. Consequently, 42 springs are used along the pile length with the interval to be 1000 mm. The basic soil parameters needed for calculating the values of the  $p$ - $y$  curve are listed in Table 5. Finite

Table 6 The selected earthquake ground motions

Earthquake Name	Date	Station	Magnitude	Distance (km)	PGA	Scaled factor
Imperial Valley	1940	EL-Centro	6.95	6.09	0.34g	0.73
Taft-69 Deg	1952	Lincoln School	7.36	38.89	0.16g	1.56
Landers	1992	Joshua Tree	7.28	11.03	0.29g	0.86
San Fernando	1971	Palmdale Fire Station	6.61	28.99	0.27g	1.08
Taft-339 Deg	1952	Lincoln School	7.36	38.39	0.18g	1.38
Loma Prieta	1989	Anderson Dam	6.9	20.26	0.48g	1.93

Table 7 Seismic responses of the bearing under earthquake excitations

Ground motion	Longitudinal displacement (mm)			Shear force (kN)		
	FPS	DCFP	TFPS	FPS	DCFP	TFPS
EL-Centro	115.9	222.8	209.3	2653	2247	2301
Taft-69Deg	220.7	221.2	223.1	3648	2203	2372
Landers	98.0	125.5	111.1	2453	1758	1640
San Fernando	131.5	175.8	181.5	2833	2064	2073
Taft -339 Deg	117.9	207.5	215.0	2683	1851	2347
Loma Prieta	98.2	137.2	164.4	2464	1811	1916
Artificial	156.7	153.7	241.4	3082	1948	2598
Mean value	134.1	177.7	192.3	2831	1983	2178

element model of the bridge established based on the abovementioned techniques is shown in Fig. 11.

## 6. Fast nonlinear analysis

Fast Nonlinear Analysis method was used in time history analysis of the bridge structure. The method is efficient, particularly for structural systems which are primarily linear elastic but have a limited number of predefined nonlinear elements. The nonlinear forces are treated as external loads and modified modal equations are formed. FNA method avoids the calculation of stiffness matrix at each time step and hence it is several magnitudes faster than the traditional nonlinear integration method. The analysis was performed with the program SAP2000, Version 14.1.0, using the Fast Nonlinear Analysis (FNA) method with a large number of Ritz vectors (140) so that the results are basically accurate.

### 6.1 Selection of the ground motions

Seismic fortification intensity of the offshore region where the prototype bridge located is 8 degree as per seismic hazard map of China. The site class of the bridge location is III, the characteristic period is  $T_g=0.65$  s, the design basic acceleration of ground motion is  $A=0.249$  g, the coefficient of seismic importance of a bridge is  $C_i=1.7$ , the coefficient of the site is  $C_s=1.2$ , the coefficient of damping modification is  $C_d=1.0$ . Design spectra is established in accordance with *Guideline for seismic design of highway bridges (JTG/T 2008)* based on the predefined parameters. Earthquake ground motions were selected by controlling average spectra values at two frequency ranges, namely, the  $0.1-T_g$  (where  $T_g$  is the characteristic period of the site) platform and the fundamental vibration period of the global bridge vibrations. The difference between a real

ground motion and the design spectra at the two frequency ranges should not exceed 10%-20%. Seven ground motions with a probability of exceedance of 5% in 120 years (P3 level) and a peak ground acceleration of 0.249 g were selected to conduct dynamic analyses. The selected earthquake ground motions are listed in Table 6 and the response spectra of selected ground motions and the design spectra are shown in Fig. 12.

### 6.2 Response results

The seven selected ground motions were input in the longitudinal direction of the offshore bridge models, which were isolated by three types of friction sliding bearings, and the seismic response of each bridge model was obtained through FNA analysis.

#### 6.2.1 Responses of the bearings

Fig. 13 shows the force-deformation behavior of the bearing under the selected ground motions. The peak displacement and shear force of the bearing are listed in Table 7.

Bi-linear behavior of FPS is observed in Fig. 13, revealing the fact that FPS begins sliding after exceeding the static friction force. Post-elastic stiffness of DCFP is smaller than that of FPS, and a second stiffness occurs in the case of large bearing displacement, indicating tri-linear behavior. Due to the existence of multiple spherical sliding surfaces, TFPS exhibits multi-linear behavior and adaptive stiffness. However, the hysteretic loop of TFPS under certain earthquake ground motion (for example Landers ground motion) is found not to exactly follow the theoretical multi-linear curves as shown in Fig. 9. This is because the displacement responses of the bearing under these ground motions are relatively smaller than the displacement limit value that is capable of changing the stiffness of the bearing.

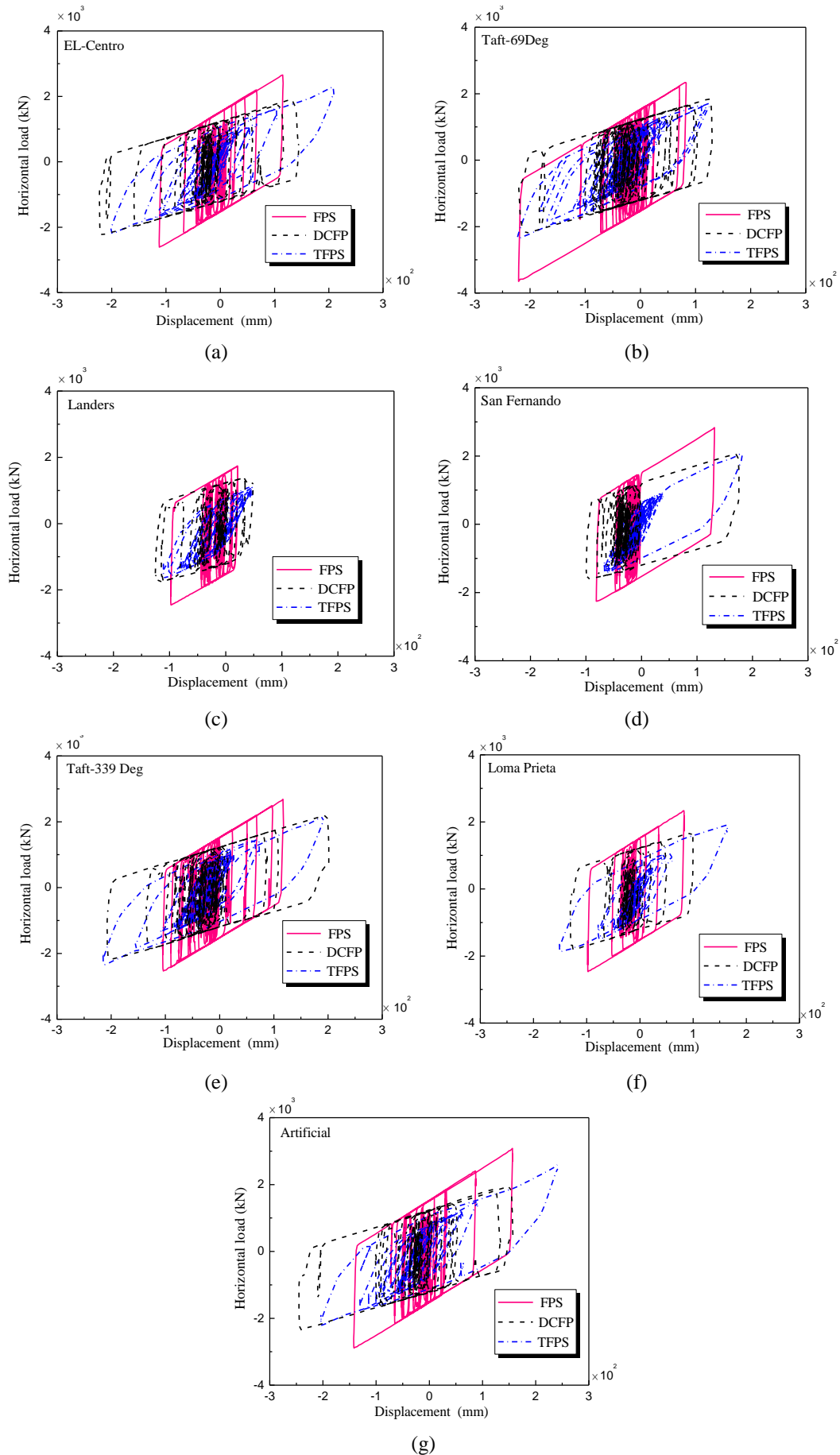


Fig. 13 Hysteretic behavior of bearings per input earthquakes

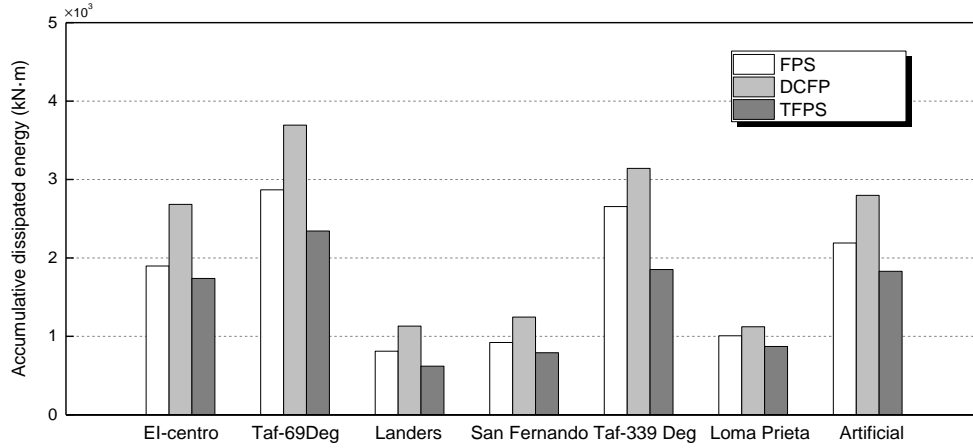


Fig. 14 Accumulative energy dissipation of the three types of bearings per input earthquakes

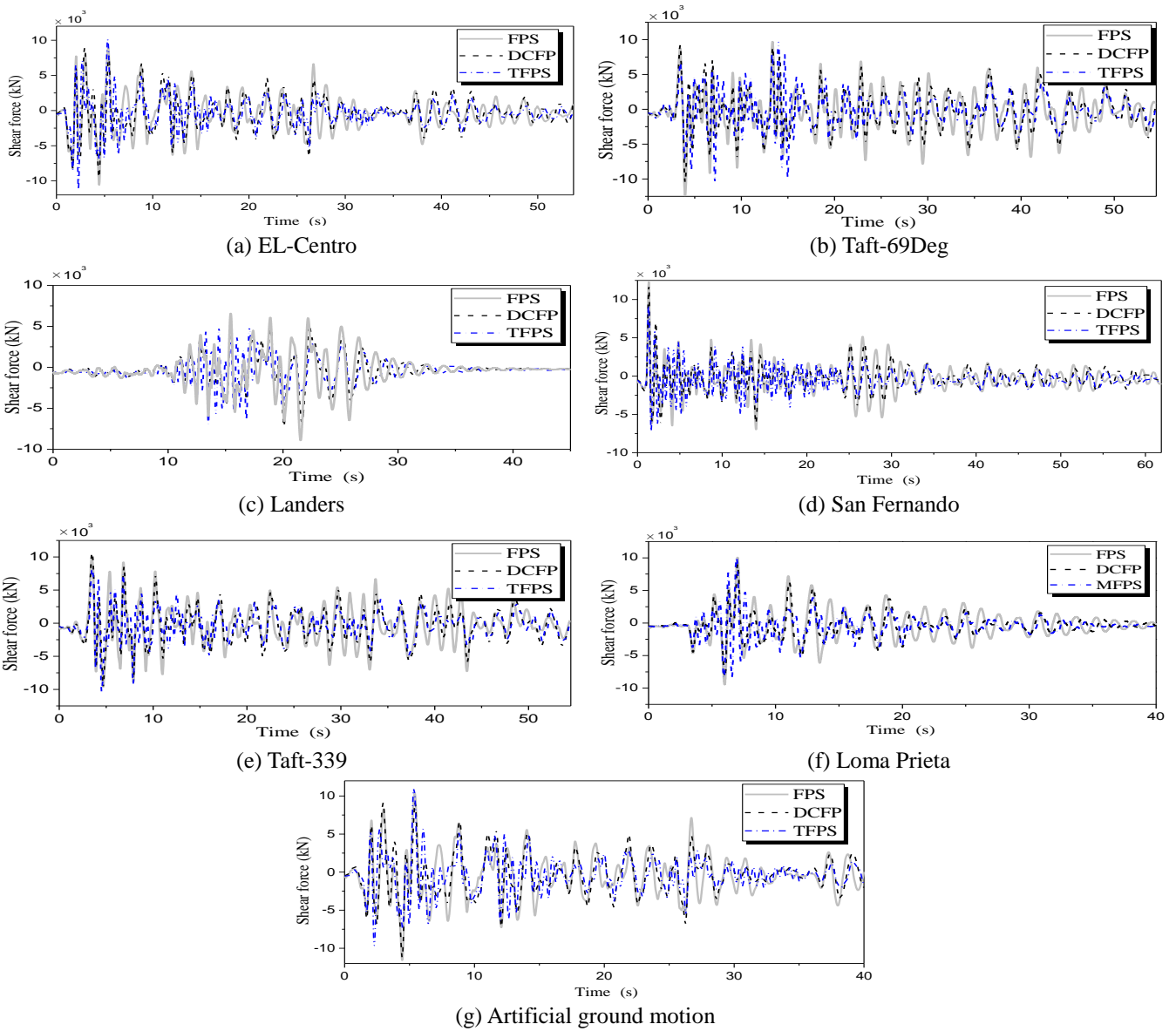


Fig. 15 Time history response of shear force of pier bottom

There are significant differences in displacement and shear force responses among the three types of bearings

when subjected to the same earthquake excitation, as demonstrated in Table 7. For instance, under the Taft-339

Table 8 Maximum response of bridge per input earthquakes

Ground motion	Shear force (kN)			Bending moment(kN·m)			Displacement(mm)		
	FPS	DCFP	TFPS	FPS	DCFP	TFPS	FPS	DCFP	TFPS
EL-Centro	10581	9489	10216	127865	117844	126061	77	71	76
Taft-69Deg	12365	10459	10456	150487	131540	126359	91	79	76
Landers	8924	7188	6887	107723	87704	83841	65	53	50
San Fernando	12295	11759	9217	150119	146943	111602	91	88	67
Taft -339 Deg	9887	10609	10390	120501	133374	124572	73	80	75
Loma Prieta	10048	9055	9118	122524	114043	113097	74	68	73
Artificial	11575	11181	10994	140635	139426	135500	85	84	82
Mean value	10810	9963	9897	131402	124563	120147	79	75	72

Table 9 Response spectrum analysis of the isolated bridge

Type	Displacement of the bearing (mm)	Shear force of the bearing (kN)	Shear force of bottom pier (kN)	Bending moment of bottom pier (kN.m)	Displacement of top pier (mm)
FPS	122.23	2629	9774	116820	70.73
DCFP	176.91	1912	7859	92503	56.20
TFPS	164.80	1856	7527	86002	52.41

Deg earthquake excitation, the displacements of FPS, DCFP and TFPS bearings are 117.9 mm, 207.5 mm, 215.0 mm, respectively. The displacement of FPS is about 56.8% and 54% of the values of DCFP and TFPS, respectively. The shear forces of FPS, DCFP and TFPS bearings are 2683 kN, 1851 kN, 2347 kN, respectively. The shear forces of DCFP and TFPS are found to be smaller than that of FPS by 31% and 13%, respectively. Great variances in displacement and shear responses of the same bearing under different earthquake excitation are also observed. The peak displacement and shear force responses of FPS subjected to Landers ground motion are 98 mm and 2453 kN, while those values under Taft-69 Deg ground motion are 220 mm and 3648 kN.

There are great variances in seismic response of the bearing when subjected to different earthquake excitations. The seismic responses of FPS, DCFP and TFPS bearings indicate that the bearing displacements of TFPS are slightly larger than those of DCFP (see Table 5). In addition, both TFPS and DCFP are capable of generating significantly larger horizontal displacements than FPS. In general, TFPS exhibits multi-linear behavior with small stiffness, DCFP exhibits tri-linear behavior with moderate stiffness, and FPS exhibits bi-linear behavior with large stiffness. Fig. 14 shows the accumulative energy dissipation of the three types of bearings. It can be seen that energy dissipation of the bearings varies greatly under different earthquake excitations. However, the energy dissipated by DCFP bearing is the largest and that of TFPS bearing is the smallest in all cases.

### 6.2.2 Responses of the bridge piers

Bridge piers, which are the main structural members of a bridge, are vulnerable when subjected to severe earthquakes. Hence, seismic response analysis of the bridge piers can better illustrate isolation effect of the three types of bearings. Fig. 15 shows the time history response of shear force of pier bottom under 7 earthquake ground motions. When subjected to the given ground motions,

reductions in seismic responses of bridge piers isolated by DCFP and TFPS bearings are observed compared to those isolated by FPS bearing. At the initial stage of earthquake excitation, shear forces of bridge piers isolated by DCFP and TFPS bearings decrease synchronously with those of FPS isolated bridge piers. While at the middle and later time of earthquake excitations, amplitude of the shear response is smaller than that of FPS isolated bridge and period shift and phase hysteresis also occur. Compared with the bridge isolated by DCFP bearings, the response amplitude of the bridge isolated by TFPS is reduced slightly and the change of vibration period is not obvious. This may be due to the low earthquake intensity that results in little or not significant displacement on number 2 and 3 surfaces of TFPS bearing, in which TFPS works as DCFP. Hence, TFPS exhibits similar behavior as DCFP.

Table 8 lists the peak responses of the bridge piers. Shear force and bending moment of the bottom of the pier and displacement of the top of the pier of the bridge with DCFP and TFPS bearings are smaller than those of bridge with FPS bearing. There is great variance in the seismic response of bridge piers when subjected to different earthquake excitations. Under San Fernando earthquake excitation, the reduction ratios for shear force, bending moment, and displacement of bridge piers utilizing DCFP bearing are 4%, 2%, 3%, respectively, while those for TFPS bearings are 29%, 25%, 26%, respectively. When subjected to the EL-Centro earthquake excitation, the shear force, bending moment, and displacement of the bridge pier utilizing DCFP bearings decrease by 10%, 8%, 8%, respectively, while those of TFPS decrease by 3%, 1%, 1%, respectively. As a whole, the seismic responses of the bridge utilizing TFPS are slightly smaller than those of the bridge utilizing DCFP bearings. However, increases on the seismic responses of bridge isolated by DCFP and TFPS bearings are observed compared with those of the bridge isolated by FPS bearing when subjected to the Taft-339 Deg earthquake excitation. The shear force, bending moment and displacement responses of the bridge using DCFP

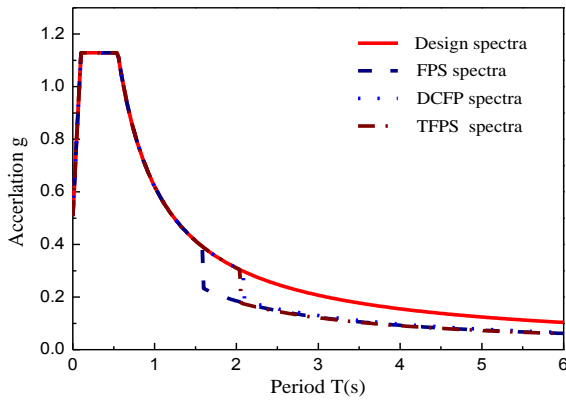


Fig. 16 Acceleration spectrum in multi-mode analysis

increase by 7%, 11%, 10%, respectively. From the above results, differentiation of seismic responses of the bridge structure are observed, which is due to the influence of spectral characteristics of selected ground motions. This needs to be considered in the selection of isolation bearings in bridge seismic design.

From the above analysis, it can be concluded that the isolation effect of TFPS is better than DCFP and DCFP is better than FPS under the given basic parameters of the bearing. However, discreteness is observed in seismic responses, therefore optimization and regression analysis need to be carried out in engineering applications.

## 7. Response spectrum analysis

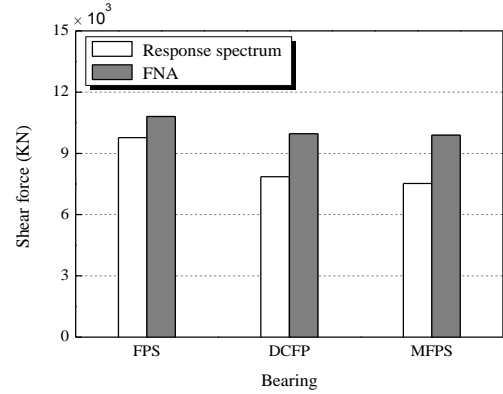
### 7.1 Equivalent linearization

In the equivalent linearization method, the behavior of isolators is modelled by linear elastic elements with the stiffness equal to the effective or secant stiffness of the element at the actual displacement. The effect of energy dissipation of the isolation system is considered by representing the isolators with equivalent linear viscous elements based on the energy dissipated per cycle at the actual displacement. The response is then calculated by using the response spectra that are modified for the effect of damping larger than 5% through damping reduction factor  $B$ . The damping reduction factor  $B$  is a function of the damping ratio. Formulas to calculate factor  $B$  are given in various codes and specifications. The values of factor  $B$  recommended by Eurocode8 (2005) is given as follows:

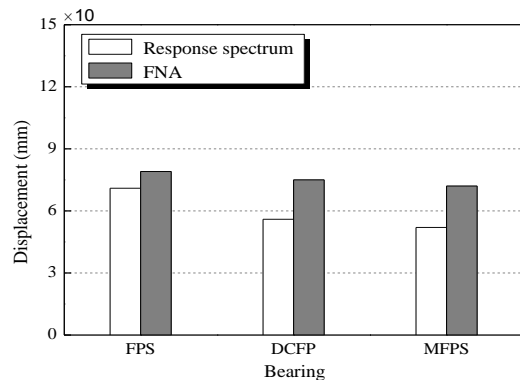
$$B = \sqrt{\frac{0.05 + \xi}{0.10}} \quad (9)$$

where,  $\xi$  is the damping ratio.

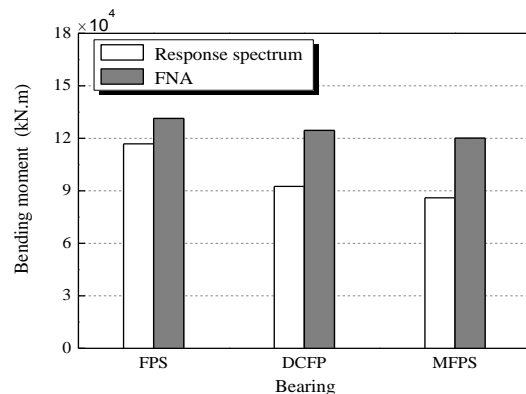
The ordinates of the 5%-damped response spectrum for values of period larger than  $0.8T_{eff}$  are divided by damping reduction factor for the effective damping of the isolated bridge. Only the isolated modes are allowed to consider the reduction of response due to increased damping. The response spectrum used in multi-mode analysis of the offshore bridge isolated with the three friction pendulum bearings is presented in Fig. 16.



(a) Shear force



(b) Displacement



(c) Bending moment

Fig. 17 Comparison between response spectrum analysis and FNA analysis

Response spectrum analysis of the equivalent linear bridge structure was conducted. The results of these analyses are presented in Table 9.

From Table 9, it can be seen that displacements reach a maximum of 176.91 mm for DCFP bearings and a minimum of 122.23 mm for the FPS bearing, and shear forces reach a maximum of 2629 kN with FPS bearings and a minimum of 1856 KN with TFPS bearings, indicating that DCFP and TFPS bearings are capable of generating larger displacements and smaller shear forces. The shear force, bending moment, and displacement of bridge with TFPS bearings are smaller than the other two cases. While, those of FPS isolated bridge are larger than the other two. All of the three kinds of isolation bearings have favorable isolation

effect. Among the three alternatives, isolation effect of TFPS is better than DCFP, and DCFP is better than FPS.

### 7.2 Comparison of response results

Fig. 17 compares results of response spectrum and FNA analysis. It can be inferred that isolation effect of the three types of friction sliding isolators obtained by response spectrum analysis is consistent with that by FNA analysis. The resulting shear forces and bending moments of the pier bottom, as well as the displacements of the pier top are in all cases greatest for the FPS and smallest for the TFPS. Seismic responses of the isolated bridge obtained by response spectrum analysis are 20% smaller than those from FNA analysis. This can be attributed to the ignorance of the influence of higher mode shapes in the equivalent linearization.

## 8. Conclusions

This paper investigates the effectiveness of three sliding-type bearings as seismic isolation for offshore bridges. Both experimental and numerical investigations of the bridge isolated with sliding-type bearings were carried out. Response spectrum and fast nonlinear analysis methods are employed to investigate the seismic response of bridges isolated with FPS, DCFP, and TFPS bearings, considering the soil-structure interaction effect. The following conclusions can be drawn from the experimental and analytical results:

- The experimental and numerical results of the shake table tests demonstrate a substantial reduction of seismic response of isolated bridge in comparison with the non-isolated bridge, and favorable isolation effect is provided by the FPS bearing.
- Isolation effect of the three types of friction sliding isolators obtained by response spectrum analysis is consistent with that by FNA analysis. However, seismic responses of the isolated bridge obtained by response spectrum analysis are 20% smaller than those from FNA analysis. Analytical results reveal that FPS, DCFP, and TFPS reduce seismic responses of the bridge and all exhibit satisfactory isolation effects.
- The three sliding-type bearings can effectively reduce the earthquake influence on bridge substructures. However, there is significant variance in the isolation effect of the three kinds of bearings with the same dimension and friction coefficient. Under the same earthquake excitation, TFPS and DCFP bearings are capable of generating larger displacements and smaller shear force. By comparing shear forces and bending moments of the pier bottom and displacements of the pier top, it can be inferred that isolation effect of the TFPS is the best. Seismic responses of the bridge piers isolated by TFPS and DCFP are smaller than those of bridge piers isolated by FPS. Discreteness is observed in seismic responses, therefore optimization and regression analysis need to be carried out in the selection of the of isolation bearings in bridge seismic design.

## Acknowledgments

This research is funded by the National Natural Science Foundation of China (NSFC) (Grants No.51478022, No.51678014) and the Fundamental Research Funds for the Central Universities (Grants No.3142016006, NO.3142018014). These supports are gratefully acknowledged. The results and conclusions presented in the paper are those of the authors and do not necessarily reflect the view of the sponsors.

## References

- Amiri, G.G., Shalmaee, M.M. and Namiranian, P. (2016), "Evaluation of a DDB design method for bridges isolated with triple pendulum bearings", *Struct. Eng. Mech.*, **59**(5), 803-820. <http://dx.doi.org/10.12989/sem.2016.59.5.803>.
- API RP 2A -WSD (2000), Recommended Practice for Planning, Design and Constructing Fixed Offshore Platforms, American Petroleum Institute, Washington, USA.
- Billah, A.H.M.M. and Alam, M.S. (2016), "Performance-based seismic design of shape memory alloy-reinforced concrete bridge piers. I: Development of performance-based damage States", *J. Struct. Eng.*, **142**(12), 04016140. [https://doi.org/10.1061/\(ASCE\)ST.1943-541X.0001458](https://doi.org/10.1061/(ASCE)ST.1943-541X.0001458).
- Castaldo, P., Palazzo, B. and Vecchia, P.D. (2015), "Seismic reliability of base-isolated structures with friction pendulum bearings", *Eng. Struct.*, **95**, 80-93. <https://doi.org/10.1016/j.engstruct.2015.03.053>.
- Catalán, A. and Foti, D. (2015), "Multilevel performance-based procedure applied to moderate seismic zones in Europe", *Earthq. Struct.*, **8**(1), 57-76. <http://dx.doi.org/10.12989/eas.2015.8.1.057>.
- Constantinou, M.C. (2004), "Friction pendulum double concave bearing", NEES Report, the University at Buffalo, New York, USA.
- Du, X.L. (2016), "Earthquake damage mechanism and life-cycle performance design and control of the offshore traffic infrastructure engineering", Research Report of National Program on Key Basic Research Project of China, Beijing University of Technology, Beijing, China.
- Eurocode 8 (2005), EN1998-2, draft, Design of Structures for Earthquake Resistance, Part 2: Bridges, European Committee for Standardization, Brussels, Belgium.
- Fadi, F. and Constantinou, M.C. (2010), "Evaluation of simplified methods of analysis for structures with triple friction pendulum isolators", *Earthq. Eng. Struct. Dyn.*, **39**(1), 5-22. <http://dx.doi.org/10.1002/eqe.930>.
- Faramarz, K. and Montazar, R. (2010), "Seismic response of double concave friction pendulum base-isolated structures considering vertical component of earthquake", *Adv. Struct. Eng.*, **13**(1), 1-14. <https://doi.org/10.1260/1369-4332.13.1.1>.
- Fenz, D.M. and Constantinou, M.C. (2006), "Behaviour of the double concave friction pendulum bearing", *Earthq. Eng. Struct. Dyn.*, **35**, 1403-1424. <http://dx.doi.org/10.1002/eqe.589>.
- Fenz, D.M. and Constantinou, M.C. (2008a), "Spherical sliding isolation bearings with adaptive behavior: theory", *Earthq. Eng. Struct. Dyn.*, **37**, 163-183. <http://dx.doi.org/10.1002/eqe.751>.
- Fenz, D.M. and Constantinou, M.C. (2008b), "Spherical sliding isolation bearings with adaptive behavior: experimental verification", *Earthq. Eng. Struct. Dyn.*, **37**, 185-205. <http://dx.doi.org/10.1002/eqe.750>.
- Fenz, D.M. and Constantinou, M.C. (2008c), "Modeling triple friction pendulum bearings for response-history analysis", *Earthq. Spectra*, **24**(4), 1011-1028.

- <http://dx.doi.org/10.1193/1.2982531>.
- Han, Q., Du, X.L., Liu, J.B., Liu, Z.X., Li, L.Y. and Zhao, J.F. (2009), "Seismic damage of highway bridges during 2008 Wenchuan earthquake", *Earthq. Eng. Eng. Vib.*, **8**(2), 263-273. <http://dx.doi.org/10.1007/s11803-009-8162-0>.
- Han, Q., Liu, W.G. and Du, X.L. (2012), "Computational model and experimental validation of multi-spherical sliding friction isolation bearings", *Chin. J. Highw. Transp.*, **25**(5), 82-88. <http://dx.doi.org/10.19721/j.cnki.1001-7372.2012.05.013>.
- Heidari, M., Jahanandish, M., Naggari, H.E. and Ghahramani, A. (2014), "Nonlinear cyclic behavior of laterally loaded pile in cohesive soil", *Can. Geotech. J.*, **51**(2), 129-143. <http://dx.doi.org/10.1139/cgj-2013-0099>.
- JTG/T B02-01-2008, Guideline for seismic design of highway bridges, Ministry of Transport of the People's Republic of China; Beijing China.
- Kang, Q., Huang, X.Y., Chen, J.Q. and Zhou, L. (2014), "Seismic response analysis of multi-span continuous isolated bridge", *Earthq. Eng. Eng. Dyn.*, **34**(1), 217-223. <http://dx.doi.org/10.13197/j.eeev.2014.01.217.kangq.029>.
- Kim, Y.S. and Yun, C.B. (2007), "Seismic response characteristics of bridges using double concave friction pendulum bearings with tri-linear behavior", *Eng. Struct.*, **29**, 3082-3093. <http://dx.doi.org/10.1016/j.engstruct.2007.02.009>.
- Matlock, H. (1970), "Correlations for design of laterally loaded piles in soft clay", *Proceedings of 2nd Offshore Technology Conference*, Houston, USA.
- Peng, T.B. and Wu, Y.C. (2017), "RTS test study and numerical simulation of mechanical properties of HDR bearings", *Earthq. Struct.*, **13**(3), 299-307. <http://dx.doi.org/10.12989/eas.2017.13.3.299>.
- Saha, A., Saha, P. and Patro, S.K. (2018), "Seismic protection of the benchmark highway bridge with passive hybrid control system", *Earthq. Struct.*, **15**(3), 227-241. <http://dx.doi.org/10.12989/eas.2018.15.3.227>.
- Tsai, C.S., Chen, W.S., Chiang, T.C. and Chen, B.J. (2006), "Component and shaking table tests for full-scale multiple friction pendulum system", *Earthq. Eng. Struct. Dyn.*, **35**, 1653-1675. <http://dx.doi.org/10.1002/eqe.598>.
- Tsai, C.S., Lin, Y.C. and Su, S.C. (2010), "Characterization and modeling of multiple friction pendulum isolation system with numerous sliding interfaces", *Earthq. Eng. Struct. Dyn.*, **39**, 1463-1491. <http://dx.doi.org/10.1002/eqe.1044>.
- Zayas, V.A., Low, S.S. and Mahin, S.A. (1987), "The FPS earthquake resisting system", Rep. No. UCB/ EERC-87/01; Earthquake Engineering Research Center, Univ. of California at Berkeley.